Nuclear Inst. and Methods in Physics Research, A 957 (2020) 163420

Contents lists available at ScienceDirect

Nuclear Inst. and Methods in Physics Research, A

journal homepage: www.elsevier.com/locate/nima

The CLAS12 Low Threshold Cherenkov detector

M. Ungaro [a,*], D. Anderson [a], G. Asryan [a], M.A. Antonioli [a], P. Bonneau [a], V.D. Burkert [a], S. Christo [a], M. Cook [a], B. Duran [b], B. Eng [a], A. Hoebel [a], D. Insley [a], J. Jacobs [a], S. Joosten [c], M. Leffel [a], T. Lemon [a], M. McMullen [a], Z.E. Meziani [b,c], R. Miller [a], P.B. Rojas [a], Y.G. Sharabian [a], A. Yegneswaran [a]

[a] Thomas Jefferson National Accelerator Facility, Newport News, VA 23606, USA
[b] Temple University, Philadelphia, PA 19122, USA
[c] Argonne National Laboratory, Lemont, IL 60439, USA

ARTICLE INFO

Keywords:
Electron scattering
Hadronic physics
Cherenkov
Mirrors
Reflectivity
Alignment
Photoelectron

ABSTRACT

The CLAS Cherenkov threshold gas detector was instrumental for electron identification in the Hall B 6 GeV era at Jefferson Lab. The detector's scope has been modified for the new CLAS12 spectrometer to identify π^+ and π^- for momenta greater than 3.5 GeV, thus becoming a Low Threshold Cherenkov Counter (LTCC). This was accomplished with a refurbishment of the gas container, its windows, mirrors, Winston light collecting cones, and photomultipliers. The design, construction, and performance of the refurbished LTCC are described. The lightweight mirrors and Winston cones have been re-surfaced with a highly reflective coating, the 5-in photomultiplier tube entrance windows have been treated with p-terphenyl to enhance the ultraviolet response, and the gas volume has been expanded to increase the thickness of the radiator gas and correspondingly the number of photoelectrons in the response signal. The LTCC response calibration has been performed on the single photoelectron signals, and the system efficiencies and response functions have been measured.

1. Introduction

The CEBAF Large Acceptance Spectrometer for operation at 12 GeV beam energy (CLAS12) [1] in Hall B at the Jefferson Laboratory (JLab) was designed to study electro-induced nuclear and hadronic reactions by providing efficient detection of charged and neutral particles over a large fraction of the full solid angle. CLAS12 is based on two superconducting magnets and multiple detector subsystems that provide large coverage for the detection of charged and neutral particles produced by the interaction of the electron beam from the JLab CEBAF accelerator with a target located at the center of the spectrometer.

A six-coil torus magnet [2] defines the six-sector structure of the so-called Forward Detector that is outfitted with Drift Chambers [3] for charged particle tracking and multiple detector systems for particle identification. These detectors include threshold Cherenkov Counters (which includes the Low Threshold Cherenkov Counter and the High Threshold Cherenkov Counter [4]) and Ring Imaging Cherenkov Counters [5], scintillator-based time-of-flight hodoscopes [6], and electromagnetic calorimeters [7]. In the target region, a 5 T superconducting solenoid [2] surrounds the Central Vertex Tracker based on silicon and micromegas detectors [8,9], and subsystems for particle identification that include a time-of-flight scintillation counter barrel [10] and a neutron detector [11], forming the so-called Central Detector.

A model representation of the CLAS12 spectrometer identifying the Forward and Central Detectors is shown in Fig. 1. In between the central and forward region, the CLAS12 Forward Tagger [12] extends the kinematic coverage for the detection of electrons and photons at polar angles from 2° to 5°. The total number of readout channels of CLAS12 is larger than 100k. Typical trigger rates are 15 kHz. In 2018, data rates of 500 MB/s with a live time of >95% were achieved.

The spectrometer has met the performance criteria for operation at an instantaneous luminosity up to 10^{35} cm^{-2} s^{-1} and momentum resolution σ_p/p in the forward direction using the drift chambers and in the central direction using the vertex tracker of <1% and <3%, respectively.

1.1. LTCC original design and performance

The CLAS Cherenkov detector [13] was instrumental in identifying electrons in the CLAS spectrometer in Hall B during the Jefferson Lab 6 GeV era. It was used to provide electron/pion discrimination with an efficiency >90%.

The system consisted of identical detectors in each of the six sectors on the CLAS Forward Carriage, each containing:

- 108 lightweight adjustable mirrors;

* Corresponding author.
E-mail address: ungaro@jlab.org (M. Ungaro).

https://doi.org/10.1016/j.nima.2020.163420
Received 13 December 2019; Accepted 7 January 2020
Available online 10 January 2020
0168-9002/

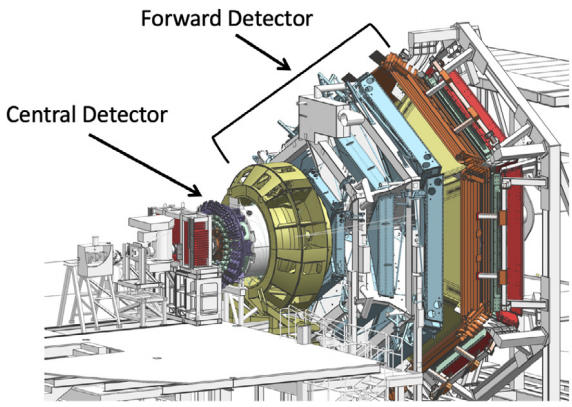

Fig. 1. Model representation of the CLAS12 spectrometer in Hall B at JLab. The electron beam is incident from the left side of this figure. The CLAS12 detector is roughly 20 m in scale along the beam axis. The CLAS12 Forward and Central Detectors are identified.

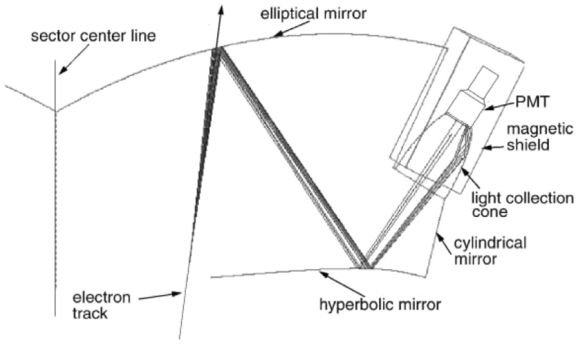

Fig. 2. Arrangement of one of the 216 modules of the CLAS Cherenkov detector, showing the optical and light collection components.

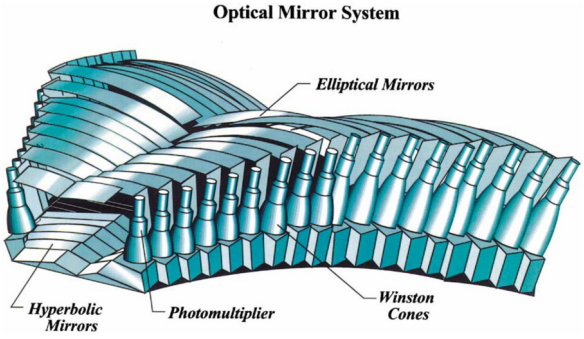

Fig. 3. A diagram of the array of optical modules in one Cherenkov detector, highlighting the main system components.

- 36 Winston light collecting cones coated with p-terphenyl;
- 36 5-in Photonis X4500B PMTs;
- 36 passive magnetic shields;
- C_4F_{10} gas, index of refraction: 1.00134.

The optics of each module was designed to focus the Cherenkov light onto a photomultiplier tube (PMT) associated with that module and located in the region obscured by the CLAS torus magnet coils. Fig. 2 shows the optical arrangement of one module. The array of the modules in one sector is shown in Fig. 3.

The detector was operational for about 17 years. The typical number of photoelectrons detected for an electron passing through the detector volume was between 10 and 20. The PMT nominal gain produced a signal too small to be digitized by the CLAS12 readout ADC and TDC electronics and thus needed an additional ×10 multiplier module. The detector had several issues that affected the optics and system efficiency. It had significant gas leaks, the mirror misalignments led to inefficiencies that reduced the signal strength, and the mirror supports were broken in several places in all sectors.

Table 1
The momentum coverage of the refurbished LTCC to provide for charged pion/kaon discrimination. The top row indicates the particle momenta in GeV. The highlighted boxes indicate the range for which particles produce a signal in the LTCC. The pion/kaon discrimination is provided from about 3.7 to 8.5 GeV.

	1	2	3	4	5	6	7	8	9	10
e										
π										
k										

1.2. Detector upgrade

With the 12 GeV energy upgraded accelerator [14], the momentum of the particles in Hall B increases substantially. Given the pion Cherenkov threshold of 2.6 GeV, the detector cannot provide a good electron/pion discrimination for most energies and a new High Threshold Cherenkov Counter (HTCC) [4] with a CO_2 gas system has been built to provide electron discrimination up to momenta of 4.9 GeV.

The heavier C_4F_{10} gas can still be used to discriminate pions from kaons (see Table 1), thus the detector was refurbished to a Low Threshold Cherenkov Counter (LTCC). The individual detector modules have been modified to:

- Support the new scope of pion/kaon discrimination;
- Address the gas leaks and other hardware issues.

2. Requirements

The LTCC requirements to allow for an adequate pion/kaon discrimination include:

- Maximizing the polar angle coverage in each of the six sectors up to angles of 30°;
- Minimizing the radiation length in the active area of CLAS12;
- Fitting the LTCC modules in the available space between the Drift Chambers [3] and the Forward Time-Of-Flight system [6];
- Producing a signal for pions in the momentum range 4 – 8 GeV.

The radiation length of the detector was minimized in the original CLAS design by placing the light collecting cones and PMTs in the regions obscured by the torus magnet coils. In the active area the window radiation length is 0.02%. However, the achieved azimuthal and polar angle coverage for these counters has been slightly reduced in CLAS12 as the distance between the target and the LTCC was increased by about 2 m compared to the CLAS configuration. This brought some of the passive elements of the LTCC into the active area of the detectors behind it, namely the support structure of the mirrors, the Winston cones, the PMT magnetic shields, and the detector walls. The remaining requirements to allow for adequate pion/kaon separation of the LTCC system have been addressed by the refurbishment and are discussed in this paper.

3. LTCC refurbishment

The re-scoping of the LTCC to discriminate pions instead of electrons required a dramatic increase in the number of photoelectrons detected. Four areas were considered to achieve this:

1. Increase optical reflectivity;

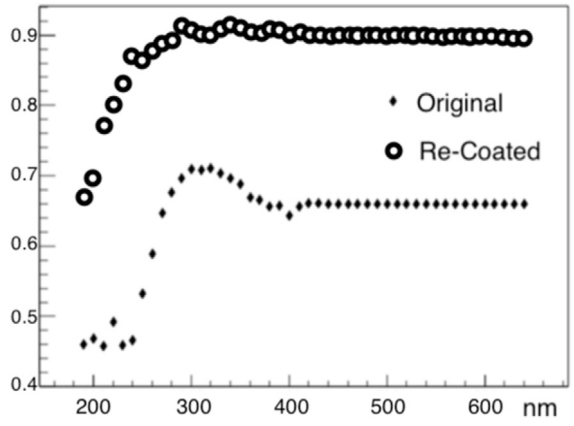

Fig. 4. Typical reflectivity vs. wavelength measurement results of one original LTCC mirror (diamonds) shows a 65% reflectivity compared to what is achieved by a new coating (open circles), about 90% reflectivity. The increase is even greater at smaller wavelengths.

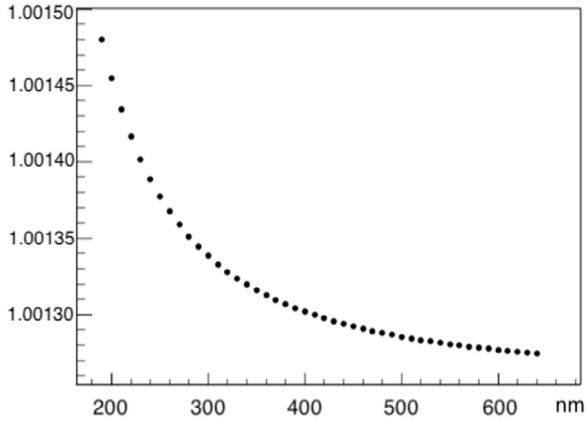

Fig. 5. The C_4F_{10} gas index of refraction as a function of wavelength.

2. Increase PMT response to ultraviolet (UV) light;
3. Increase radiator gas thickness;
4. Address the gas leaks and other hardware issues.

Monte Carlo simulations of pions in the LTCC quantified the number of Cherenkov light reflections on the cylindrical, elliptical, parabolic, and Winston cone surfaces as:

- 2 reflections only: 30% of the events;
- 3 reflections: 40% of the events;
- 4 or more reflections: 30% of the events.

These results were confirmed by measurements of the relative amount of laser light reflected by the mirror surfaces to the face of the PMTs during the mirror alignment.

A study of the refurbishment of the mirror and Winston cone surfaces led to re-coating studies using several vendor companies. The original average measured reflectivity of the mirrors and Winston cones showed a degraded reflectivity when compared to the original values obtained at installation and to the new coated samples, due to 17 years of aging, see Fig. 4.

In the study, a few scenarios using the C_4F_{10} index of refraction (shown in Fig. 5) and considering the various reflection probabilities outlined above were compared:

- using old or new mirror reflectivity (see Fig. 4);
- using a completely transparent gas or the C_4F_{10} with its measured transparency;

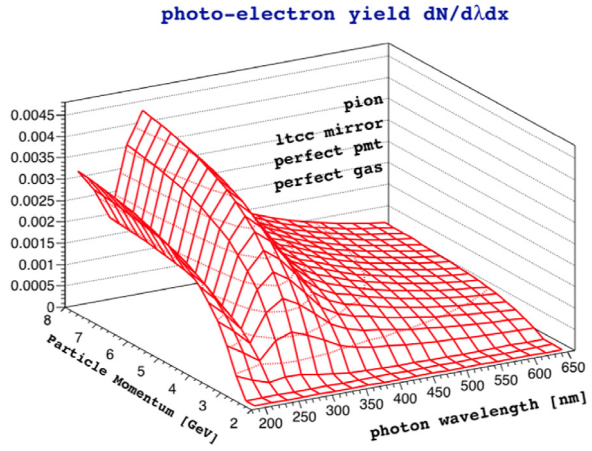

Fig. 6. Cherenkov light yield as a function of pion momentum and photon wavelength using the Frank–Tamm formula for one of the scenarios considered: mirrors and Winston cones with low reflectivity (LTCC original mirror, not refurbished), a perfectly transparent gas, and an ideally refurbished PMT.

- using the actual or the enhanced PMT quantum efficiency function;
- using or not using the additional C_4F_{10} gas volume;
- comparing the pion response to the original CLAS 6 GeV era electron response.

The results of these studies are discussed below.

The reflection probability vs. wavelength distributions for each scenario was input into the Frank–Tamm formula [15] to calculate the Cherenkov radiation yield as a function of wavelength and momenta:

$$\frac{d^2n}{dxd\lambda} = \frac{2\pi z^2\alpha}{\lambda^2}\sin^2\theta_C(\upsilon), \tag{1}$$

where α is the fine structure constant, θ_C is the Cherenkov emission angle, z is the particle charge, and υ is its speed.

The results of one particular combination among the described scenarios are given in Fig. 6 for pions, the measured non-refurbished mirror reflectivity, a 100% transparent gas, and a PMT with ideal refurbished quantum efficiency.

When the number of reflections is taken into account, the refurbished components provide a factor of 2.5 gain in the visible light wavelengths and a factor of 3.8 in the UV range:

- Visible light wavelength range:
  - original integrated reflectivity: 27.5%
  - refurbished integrated reflectivity: 68.1%
- Ultraviolet light wavelength range:
  - original integrated reflectivity: 9.1%
  - refurbished integrated reflectivity: 34.3%

The results are summarized in Fig. 7 for the two main scenarios: mirrors are re-coated and the PMT quantum efficiency is improved. By performing both of these improvements, the study shows that the LTCC response to pions will be the same as it was for electrons above 4 GeV in the original Cherenkov detector for CLAS.

The design changes of the LTCC are summarized below and discussed in the following sections:

1. Resize the box to efficiently fit in the space between the Drift Chambers and the Forward Time-Of-Flight counters:
   (a) Trim sides of the boxes
   (b) Relocate the three mirror sets closest to the back-wall

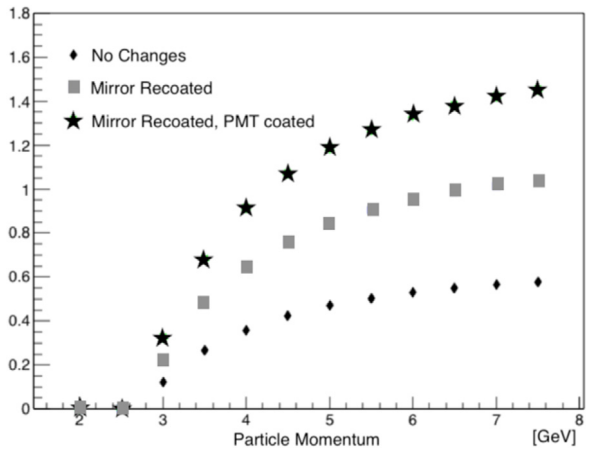

Fig. 7. Ratio of the predicted pion detection response of the LTCC to the electron detection response obtained in the old CLAS detector. Diamonds: with no refurbishment, the goal of detecting pions cannot be reached. More than a factor of two can be gained by re-coating the mirrors and Winston cones (squares). In addition, by increasing the PMT response to UV light (stars), the LTCC can now reach a performance for pions with momenta above 4 GeV that was achieved for electrons.

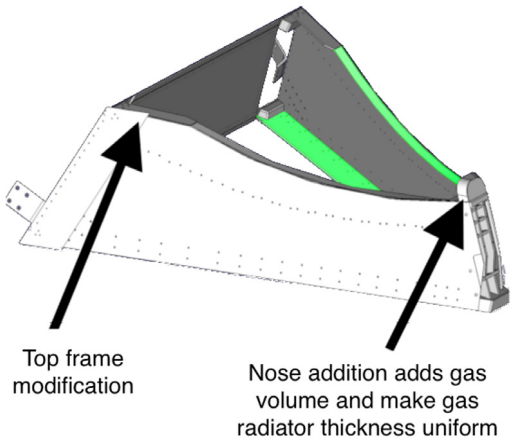

Fig. 8. The refurbished LTCC box frame. Originally the frame walls spanned a portion of the surface of a 5-m cylindrical profile. The side-walls had to be cut near the top part of the frame and the mirror sets involved had to be relocated. A stainless steel nose window support was added to the original detector to increase the gas volume. The radiator gas thickness was consequentially smaller near the top frame modifications, however the old restriction of the window having to follow the cylindrical profile of the wall was removed and the window can be inflated to follow the flat profile from the bottom of the box to the nose. This leads to the gas radiator thickness increase detailed in Fig. 9.

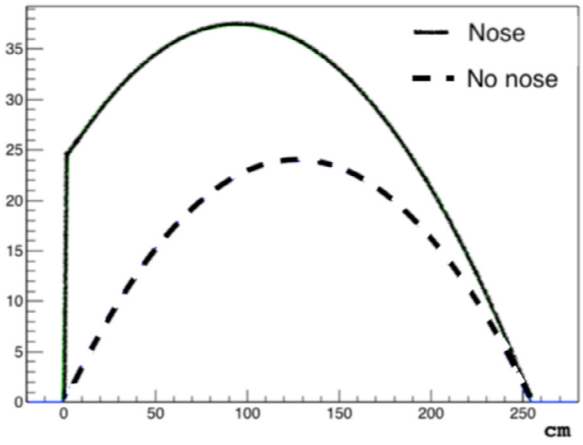

Fig. 9. The gas volume percentage gains with and without the nose addition compared to the old CLAS configuration as a function of distance from the nose in cm. Dashed: the percentage increase due to the window inflation compared to the original flat design. Solid: the additional percentage increase due to the nose addition.

(c) Redesign and replace the back-wall frame

2. Decrease inefficient regions
3. Increase PMT gain and split the output to provide both ADC and TDC signals
4. Minimize gas leaks
5. Improve the mirror supports
6. Increase light yield:

   (a) Re-coat all mirrors
   (b) Re-coat Winston cones
   (c) Wavelength shifting re-coating of the PMTs
   (d) Modify small angle nose to increase the gas volume

3.1. Box cut and support relocation

The modification of the LTCC vessel design was necessary because all of the drift chambers in the CLAS12 spectrometer are flat as opposed to the drift chambers in CLAS that were of cylindrical shape. Therefore the inlet of the LTCC vessel had to be modified from the original cylindrical to a flat profile, (see Fig. 8). As a consequence of such a modification, the possibility of a significant increase of the radiator gas thickness in the most important polar angular range of particle acceptance at small angles was considered and successfully implemented. The mounting structure of the three mirror sets involved in the cut was repositioned. For this work, new threaded holes were drilled in the frame and the old holes were plugged and sealed.

3.2. Nose addition and window inflation

In the original design the upstream window followed the cylindrical curvature of the frame side-walls. In the new system, the window is designed to inflate to enlarge the gas volume in order to increase the number of Cherenkov photons. In addition, a “nose” support (see Fig. 8) has been engineered to increase the gas volume. The nose dimensions have been optimized to provide the necessary support, while at the same time, maximizing the gas volume increase. The gas volume increase of the final configuration is shown in Fig. 9.

3.3. Back-wall and connectors

Both the high voltage and the signal connectors that link the PMTs inside the LTCC box and the outside electronics were not hermetic during CLAS operations and epoxy was used to minimize the leaks from these connectors. As part of the back-wall refurbishment, the patch panel was rebuilt and hermetic connectors were used.

The new lightweight back-wall design is shown in Fig. 10. The wall is supported by stainless steel bars that enclose a panel made of foam enclosed by thin aluminum sheets to minimize the radiation length. The new patch panels provide 3 connectors for each PMT: one for high voltage and two for the identical signals from the PMTs, due to the modifications detailed in Section 3.9. One signal is digitized through a flash ADC and the other one through a discriminator and TDC.

3.4. Mirror support spine

When the LTCC boxes were opened for refurbishment, the mirror support spine in all six Cherenkov detectors was found to be broken. The spine was an aluminum honeycomb designed to prevent mirror deformation and misalignment under their own weight. It was attached to the box nose and the back-wall. The support spine was rigid but its

Fig. 10. View of the back-wall of the refurbished LTCC box. A stainless steel bar encapsulates a sandwich of aluminum and foam. On the left and right side of the frame, new patch panels allow for 3 hermetic connectors (1 HV, 2 signals) from each PMT.

Fig. 11. The LTCC mirror support spine. The carbon fiber tube (in black) is allowed to float up to 1 cm to compensate for possible box deformations during the detector transportation and installation. The mirrors are linked to the spine through 0.127-mm thick stainless steel cables and tensioned through springs.

attachment to the box failed to withstand deformations of the box (of the order of 0.5 cm) whenever the LTCC modules were moved. A new carbon-fiber spine (see Fig. 11) was designed that is capable of floating up to 1 cm, effectively compensating for any box deformations to the modules during transportation and installation. The mirrors are linked to the spine through 0.127-mm thick stainless steel cables. The cables are anchored with stainless steel springs with tension varying from 0.5 to 1 kg.

The spine was tested by mounting a laser on the box. The laser line was focused through the elliptical and hyperbolic mirrors to a target in the middle of the covered face of a PMT. In order to verify that the detector transportation and/or installation would not break the spine or affect the mirror alignment, the box was lifted, rotated back and forth by 90°, and subjected to small vibrations. The focused spot on the PMT did not change with any of these movements and the spine compensated for the box wall deformations.

3.5. Mirror re-coating

As seen in Fig. 2, each LTCC segment is composed of four optical surfaces: three mirrors and one Winston cone. The mirrors have elliptical, cylindrical, and hyperbolic profiles in the longitudinal direction and are flat in the transverse direction. The reflectivity of a random selection of 30 elliptical, cylindrical, and hyperbolic mirrors from two sectors was measured. All of the tested mirrors showed significant degradation from the original desired reflectivity of 90% in the visible spectrum, see for example Fig. 12 (top). A refurbishment of the mirrors was crucial to enhance the detector response to pions because the intensity of their emitted Cherenkov light is greatly reduced compared to

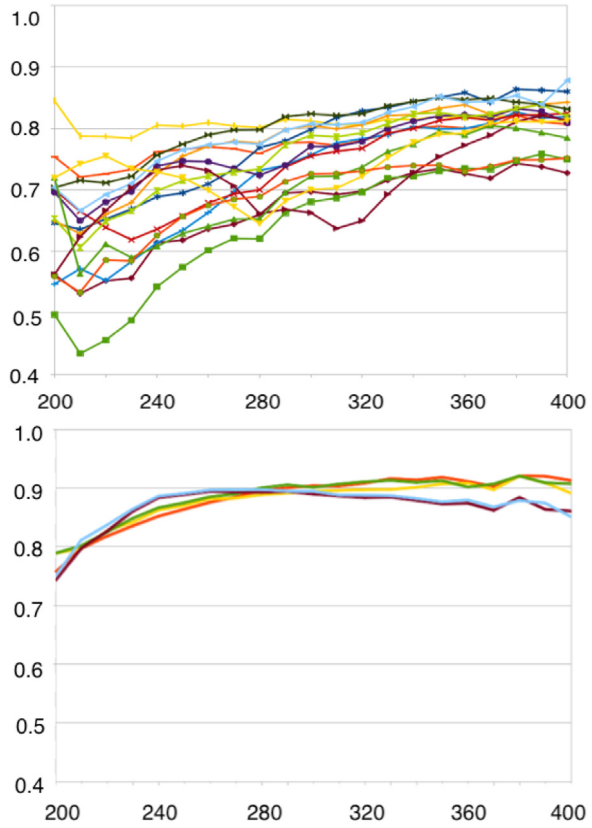

Fig. 12. Top: Reflectivity measurements as a function of wavelength for a sample of 8 mirrors before re-coating, each tested at two different places on their surface. The reflectivity was measured using a monochromator (Newport model CS260-USB-1-FH-A) with a deuterium light source with a reach between 200 nm and 400 nm. The average reflectivity was about 65% instead of the optimal 90%. Bottom: Reflectivity measurements as a function of wavelength for a sample of 5 mirrors measured after gluing on the Lexan strips (see text for details). Note the very high value of reflectivity in the UV region, where most of the Cherenkov light is produced. In the visible spectrum, the reflectivity is about 90%.

electrons, see Fig. 7 "no changes" case. Due to the material, assembly, and dimensions of the different types of mirrors, two different techniques were employed to refurbish the reflective surfaces as discussed below.

3.5.1. Re-coating of cylindrical mirrors

The cylindrical mirrors range from 6 to 12 in long. Each mirror is made from a single piece of aluminum or plastic. Due to their small size, they fit in most vacuum chambers used to coat mirrors by evaporation of aluminum with magnesium fluoride (Al+MgF_2). After successful testing of Al+MgF_2 re-coating onto the existing substrate, the work of re-coating the 216 cylindrical mirrors was awarded to ECI [16]. See Fig. 12 (bottom) for typical reflectivity values after re-coating.

3.5.2. Re-coating of elliptical and hyperbolic mirrors

The elliptical and hyperbolic mirrors are composed of a Kevlar support structure with a Lexan substrate. It was not possible to change this hardware from its original design and construction (in 1997). The support material, which allowed for pitch, roll, and yaw alignment of the mirrors, included wood and aluminum pieces that were glued to the support structure.

Several companies attempted to re-coat these mirrors but failed because the out-gassing of the mirrors' substrate materials prevented the chambers used to evaporate the coating onto the surfaces to reach the necessary vacuum levels. Furthermore, many of the mirrors are longer

than 1 m, exceeding the size of most vacuum chambers. Therefore the Al+MgF_2 could not be re-deposited directly onto the mirror substrates.

A different approach consisted of coating thin (25 μm) Lexan strips and gluing the strips onto the mirror substrates. While promising, this presented the challenge of protecting the coated Lexan strip from possible damage during shipping and handling, and during the gluing process to the mirrors.

A working chain was setup to:

1. coat the Lexan strip;
2. protect the strip with a temporary peel-able film for safe shipping and handling to JLab;
3. glue the strip to the mirror substrates;
4. remove the protective film;
5. test the reflectivity.

Several companies produced various test samples with various protective material films. The job was eventually awarded to ECI [16]. The gluing of the strips to the mirror was done at JLab. The mirrors were vacuum-mounted on a supporting structure. Loctite spray contact adhesive glue was applied on the mirror and directed out by a venting system. The strip was applied to the substrate and after 24 h of curing time the film was removed. The mirrors were monitored for shape changes due to glue joint shrinkage; none were observed during an initial test period of several days and later throughout the application of the strips to all substrates. The typical reflectivity of the refurbished mirrors is shown in Fig. 12 (bottom).

3.5.3. Elliptical mirror gaps

The LTCC elliptical mirrors, especially the longest ones, presented several gaps between the mirrors, some a few cm long. This was evident also in the data analyses as a loss of efficiency between the mirrors. To make sure that no light is lost in these gaps, additional 120-μm thick Lexan extension strips were produced and coated with Al+MgF_2. These strips were manufactured by ECI [16]. They were fitted and glued on the left side elliptical mirrors to cover the gaps (see Fig. 13).

Fig. 13. Top: the gaps between mirrors before refurbishing the LTCC. These gaps were also seeing in the data as a drop of efficiency near the middle of the detector, as the Cherenkov light was not collected. Bottom: all of the gaps are covered by the extension strips.

3.6. Mirror alignment

A new procedure was developed to align the mirrors within the LTCC boxes that takes advantage of their focusing capabilities. The elliptical mirror focal points (see Fig. 14) are 1. the target (origin of the lab coordinate system) and 2. a point behind the hyperbolic mirror. The focal points of the hyperbolic mirrors are 1. a point near the focal point of the elliptical mirrors and 2. a point above the face of the PMTs.

The geometrical shape of the mirrors has been built into the CLAS12 Geant4 simulation (called GEMC) [17]. When a laser line coming from the target is directed at the mirror, it is focused on the hyperbolic focal point, then directed at the PMT (see Fig. 14). This geometrical focusing was used during the mirror alignment: a 3 mW, 635 nm laser was placed, relative to the detector, in the center of the CLAS12 coordinate system at the location of the target, and the first ellipse focal point. The laser was mounted on a structure that allowed the beam direction and line angle to move with respect to the floor, while keeping the origin of the laser at the coordinate system origin. This position was accurate at the 0.5 mm level. The laser was spread through two cylindrical lenses into a laser line and shone longitudinally along the center-line of each elliptical mirror. Both the elliptical and hyperbolic mirrors were then adjusted in pitch, roll, and yaw to minimize the light spot dimensions and to center it in the middle of the face of the PMT. The PMT entry glasses were protected from the laser line with custom-fitted cardboard pieces. After alignment, the spot size of the laser was 5 mm.

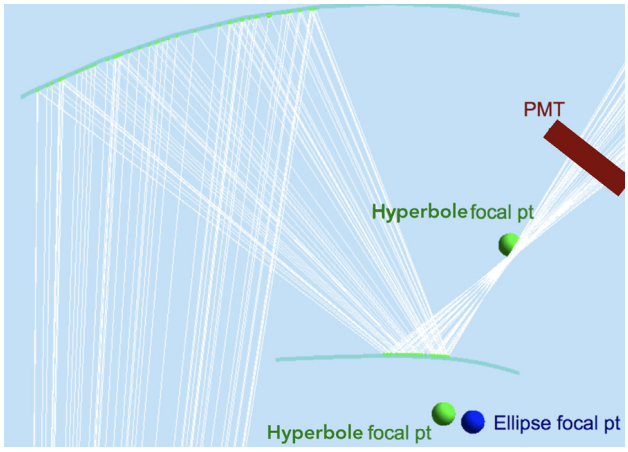

Fig. 14. The simulation of a laser line (white tracks are photons) originating from the target (first ellipse focal point) and directed at the elliptical mirrors. The photons are reflected to the second ellipse focal point. The hyperbole first focal point is near the ellipse focal point so the hyperbolic mirror reflects the incoming photons to the hyperbole second focal point, located above the face of the PMTs. This picture illustrates the procedure used for the alignment: the mirror positions were adjusted until the laser line originating from the target was focused on the face of the PMT.

3.6.1. Mirror overlap and repositioning

Two issues that could not be fixed in the refurbishment may affect the detector efficiency:

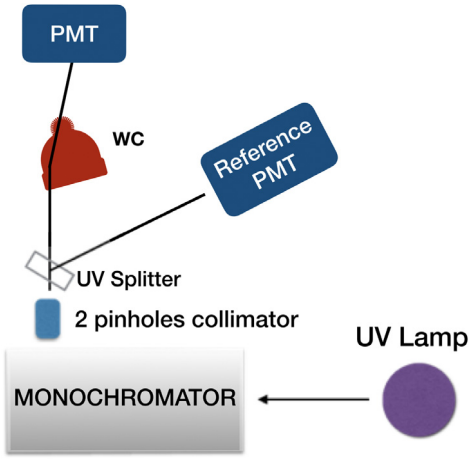

Fig. 15. Setup to measure the WC reflectivity. The wavelength of light from a deuterium lamp was measured using a monochromator and split in two beams, each with calibrated intensity. One of the beams impinged on the WC at a typical angle of 12°, while the other was directed at a reference PMT. The reflectivity was measured in different spots for a sample of WCs. The results proved to be independent of the spot location.

1. the mirrors had to be mounted following the original overlaps, see for example Fig. 13 (top). These overlaps were originally implemented to optimize the response to inbending (toward the beamline) electrons and are not optimal for outbending particles.
2. the relocation of the last four mirror sets (15, 16, 17, and 18) (mentioned in Section 3.1) may degrade the optics as the affected mirrors do not follow the optimal desired optics configuration with the target as the original focal point.

3.7. Winston cone refurbishment

Winston cones (WCs) are used to collect light onto the PMT photocathodes after one reflection. In the LTCC there are three kind of WCs:

1. Small
   (a) Height: 18 cm
   (b) Radius at the top: 20 cm
   (c) Radius at the bottom: 11 cm
   (d) Material: 0.25-cm thick copper (electro-formed)
2. Medium
   (a) Height: 22 cm
   (b) Radius at the top: 20 cm
   (c) Radius at the bottom: 11 cm
   (d) Material: 0.5-cm thick plastic (vacuum pressed)
3. Large
   (a) Height: 30 cm
   (b) Radius at the top: 22 cm
   (c) Radius at the bottom: 11 cm
   (d) Material: 0.25-cm thick copper (electro-formed)

The reflectivity of the WCs showed quantitatively the same degradation as the mirrors. However, due to their shape, re-coating of the WCs is more costly than the mirrors and the LTCC budget allowed refurbishing only 160 out of the 216 total WCs. A setup on an optical bench to measure the reflectivity for all of the WCs at wavelengths between 200 and 400 nm was designed (see Fig. 15) to accept shallow incident angles of 10°–15° (typical angles based on simulation studies).

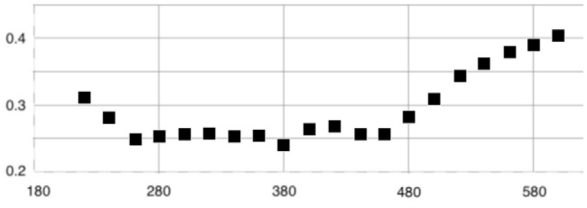

Sector 1		Sector 2		Sector 3		Sector 4		Sector 5		Sector 6	
Left	Right	Left	Right	Left	Right	Left	Right	Left	Right	Left	Right
0.67	0.30	0.67	0.70	0.56	0.56	0.51	0.81	0.40	0.44	0.72	0.80
0.26	0.36	0.62	0.59	0.64	0.63	0.86	0.65	0.37	0.37	0.77	0.38
0.70	0.45	0.64	0.65	0.38	0.71	0.42	0.51	0.33	0.39	0.50	0.47
0.33	0.27	0.79	0.76	0.57	0.76	0.75	0.64	0.32	0.81	0.46	0.41
0.32	0.27	0.70	0.72	0.71	0.51	0.73	0.69	0.45	0.65	0.89	0.24
0.57	0.45	0.69	0.65	0.59	0.61	0.55	0.78	0.33	0.42	0.44	0.57
0.31	0.49	0.68	0.65	0.71	0.81	0.75	0.83	0.40	0.41	0.37	0.54
0.33	0.459	0.53	0.56	0.76	0.76	0.78	0.74	0.43	0.50	0.52	0.32
0.69	0.54	0.47	0.78	0.67	0.75	0.74	0.72	0.45	0.47	0.55	0.47
0.33	0.30	0.68	0.71	0.71	0.75	0.68	0.83	0.08	0.39	0.42	0.44
0.78	0.59	0.79	0.80	0.77	0.76	0.64	0.74	0.77	0.68	0.77	0.75
0.77	0.72	0.56	0.77	0.76	0.71	0.73	0.74	0.60	0.90	0.75	0.80
0.23	0.73	0.72	0.69	0.46	0.48	0.72	0.68	0.69	0.75	0.50	0.64
0.51	0.59	0.59	0.44	0.43	0.53	0.63	0.46	0.62	0.68	0.44	0.66
0.47	0.70	0.49	0.71	0.63	0.48	0.82	0.64	0.65	0.70	0.67	0.42
0.72	0.66	0.72	0.77	0.75	0.66	0.71	0.52	0.70	0.70	0.57	0.62
0.66	0.74	0.78	0.43	0.59	0.64	0.52	0.71	0.54	0.69	0.19	0.66
0.77	0.54	0.78	0.74	0.76	0.63	0.63	0.66	0.69	0.55	0.69	0.59

Fig. 16. Top: typical reflectivity vs. wavelength (nm) of a "very poor" WC. The reflectivity is below 30% for most wavelengths between 200 and 400 nm. The reflectivity proved to be independent of the particular spot on the WC surface. Bottom: the average reflectivity r between 200 and 400 nm for all WCs. The shaded gray boxes represents WCs with poor reflectivity ($r < 50\%$).

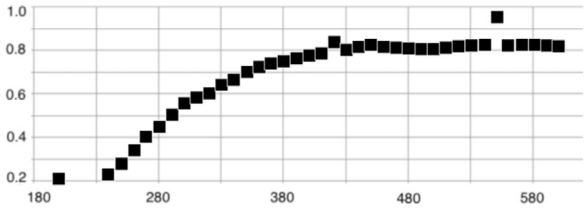

Sector 1		Sector 2		Sector 3		Sector 4		Sector 5		Sector 6	
Left	Right	Left	Right	Left	Right	Left	Right	Left	Right	Left	Right
0.67	0.81	0.67	0.65	0.77	0.56	0.51	0.81	0.86	0.81	0.81	0.80
0.74	0.83	0.85	0.59	0.64	0.69	0.86	0.65	0.85	0.85	0.77	0.82
0.70	0.84	0.64	0.65	0.83	0.73	0.85	0.73	0.73	0.81	0.82	0.79
0.75	0.78	0.79	0.76	0.57	0.76	0.84	0.77	0.54	0.81	0.80	0.84
0.81	0.80	0.71	0.82	0.81	0.84	0.75	0.69	0.86	0.80	0.89	0.81
0.86	0.83	0.69	0.65	0.81	0.81	0.78	0.78	0.82	0.84	0.79	0.57
0.80	0.86	0.68	0.85	0.81	0.75	0.69	0.83	0.81	0.81	0.83	0.79
0.87	0.459	0.75	0.80	0.74	0.76	0.78	0.78	0.84	0.81	0.85	0.82
0.69	0.80	0.84	0.78	0.67	0.75	0.76	0.72	0.82	0.84	0.84	0.86
0.83	0.30	0.82	0.71	0.81	0.75	0.68	0.83	0.08	0.78	0.80	0.81
0.78	0.59	0.79	0.80	0.77	0.76	0.64	0.66	0.77	0.56	0.77	0.75
0.77	0.68	0.56	0.77	0.52	0.71	0.65	0.68	0.60	0.90	0.65	0.80
0.34	0.82	0.72	0.85	0.53	0.50	0.89	0.68	0.70	0.75	0.50	0.75
0.51	0.66	0.70	0.44	0.48	0.55	0.63	0.46	0.62	0.67	0.44	0.66
0.77	0.75	0.48	0.73	0.63	0.48	0.82	0.64	0.65	0.68	0.67	0.42
0.86	0.91	0.81	0.77	0.82	0.81	0.69	0.52	0.89	0.67	0.45	0.62
0.73	0.82	0.78	0.53	0.78	0.72	0.52	0.75	0.54	0.76	0.80	0.66
0.77	0.58	0.78	0.86	0.68	0.68	0.55	0.79	0.73	0.55	0.62	0.84

Fig. 17. Top: typical reflectivity vs. wavelength (nm) of a "very poor" WC after refurbishment. The reflectivity quickly rises to 65% at a wavelength of about 340 nm. Bottom: average WC reflectivity r between 200 and 400 nm for all WCs. The shaded gray boxes represents WCs with poor reflectivity ($r < 50\%$). This picture should be compared to Fig. 16. Most re-coated WCs show improved reflectivity.

The typical reflectivity of a poor WC vs. wavelength is shown in Fig. 16 (top). All 216 WCs were studied, and the average reflectivity results are shown in Fig. 16 (bottom). These data allowed cataloging of the quality of the WCs to select the worst ones to refurbish. The cones were put in a vacuum chamber and Al+MgF_2 was deposited on top of the existing coating. The typical reflectivity of a representative WC after re-coating is shown in Fig. 17 (top). About 30 cones needed the additional treatment of removing the existing aluminum coating to improve the new Al+MgF_2 deposition. Even then, about half of these cones did not show improvement probably because the treatment damaged their

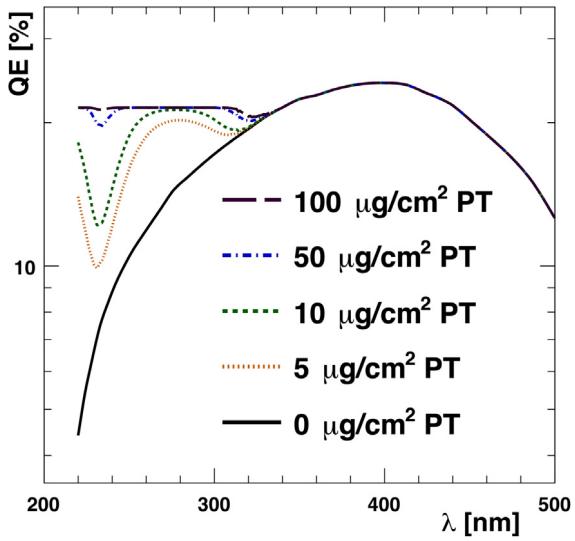

Fig. 18. The typical QE for a Photonis XP4500B PMT (solid black line), compared to the projected QE after application of a p-terphenyl wavelength shifter at four different material loads (dashed lines), as a function of wavelength.

surfaces. The results of the WC refurbishment are summarized in Fig. 17 (bottom).

3.8. PMT surface coating

The PMTs used in the LTCC are Photonis XP4500Bs [18]. Their borosilicate windows can be used to detect photons of wavelengths as low as approximately 300 nm. This is the most limiting factor of enhanced quantum efficiency (QE) in the UV region, where most of the Cherenkov light is emitted (see Eq. (1)), given that the C_4F_{10} gas is transparent down to wavelengths of 180 nm, and the mirror and WC reflectivities are non-zero even for wavelengths below 200 nm. While quartz windows maximize the UV-sensitivity of the PMT, they are fragile and expensive. A wavelength shifter (WLS) deposited on the face of a borosilicate or UV-transmitting glass PMT provides an effective alternative to boost the efficiency of a Cherenkov detector by converting UV photons with a wavelength below 300 nm into two isotropically emitted photons with longer wavelengths.

The projected QE gained by a deposition of p-terphenyl (PT) on the XP4500Bs PMT is shown in Fig. 18 [19]. The gain at shorter wavelengths near 200 nm, where most of the Cherenkov light detectable by the LTCC optics is concentrated, is more than a factor of 3.

Several tests were performed in collaboration with the Temple University Physics Department using the equipment schematics shown in Fig. 19 (top). The setup used a monochromator with a precision of 0.35 nm and two PMTs (one for the measurement, one for the reference calibration). The PMTs were switched to confirm the stability of the results. Each PMT was measured while coated and then again after the coating had been removed using acetone and isopropanol. The observed photon rate was read out by a scaler.

The results from 2 different PMTs each at 2 different positions were found to be consistent. Fig. 19 (bottom) shows the average measured gain from these four measurements. The observed gain was found to be consistent with the nominal prediction for a perfectly saturated coating.

Based on these results, 200 PMTs were treated [20] with an optimal material load of 110 μg/cm^2, corresponding to a PT thickness of 894 nm. This corresponded to an overall increase of the PMT response to Cherenkov light of about 40%. The 110 μg/cm^2 of PT provides an almost transparent coating to the visible light spectrum.

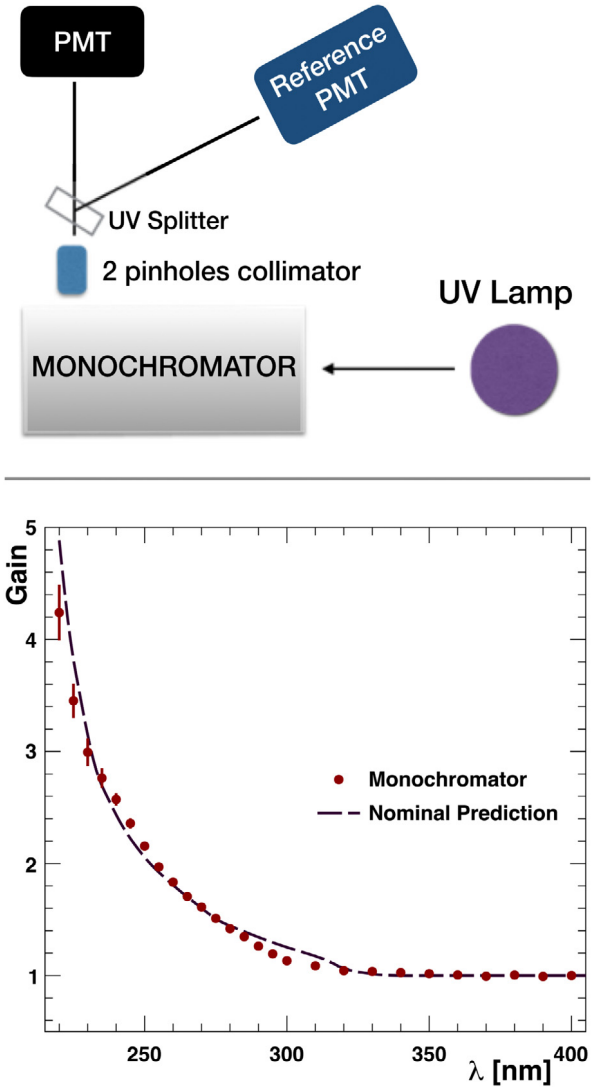

Fig. 19. Top: Monochromator setup used for the gain measurements. Bottom: Results from the monochromator measurements (red circles), compared to the nominal prediction for a p-terphenyl material load of 110 μg/cm^2 (dashed line).

3.9. PMT voltage dividers

In the original readout electronics for CLAS, the single output from each PMT was amplified by a factor of 10 and then split in two to feed the ADC and TDC boards. This amplification and splitting was performed by a dedicated electronics module (UVA 132) [13]. This unit was replaced by a pulse amplifier board entirely powered by the current flowing through the base voltage divider. This board was developed in 2002 at JLab [21].

The new electronics provided a factor of 8 to 10 PMT signal boost, while preserving the fast PMT pulse shape. It also significantly improved the signal amplitude and the signal-to-noise ratio: the high voltage needed to detect the single photoelectron signal (SPE) was reduced on average by 374 V (see Fig. 20).

The amplifier board design was adapted to use the LTCC XP4500B base and a prototype (shown in Fig. 21) was built to provide a factor of ten amplification and two identical output signals.

In Fig. 22 a comparison of the two signals shows the similarity between the two outputs. During testing of the modified PMT bases, the output was processed by a flash ADC (FADC) read out by a data acquisition system using the PMT itself as the trigger. The corresponding

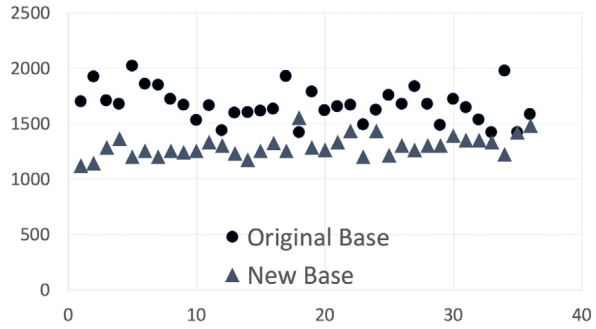

Fig. 20. Comparison of the 36 PMT high voltages (in V) in one LTCC box gain-matched to provide a SPE peak at about ADC channel 200. The PMTs with the modified bases produce the same response function as the original base but at an average voltage 374 V less (1666 V vs. 1292 V).

SPE spectrum was analyzed. The shape of the SPE signal is very similar to the original signal coming from the external dedicated splitter and amplifier through the ADC electronics shown in Fig. 22 (right).

180 bases were assembled at JLab and installed on the PMT dividers. Both signals from all of the modified bases were tested. The response of the PMTs, amplified by a factor of about 10, was verified to be identical to the original output.

3.10. The LTCC windows

The LTCC windows that cover the upstream and downstream open frame of the box are a composite of Tedlar/Mylar/Tedlar (see Fig. 23). Two layers of the Tedlar film provide reliable light tightness even if they have some defects such as wrinkles and small pinholes, while the Mylar portion adds the material strength necessary to withstand the differential gas pressure and increase wear resistance and reliability. This design, easy to handle and apply to the module, simplified the replacement of the old composite window.

The window was fabricated in two steps:

1. lamination of 1.6-m wide Tedlar/Mylar/Tedlar rolls;
2. seaming of the laminated strips into a 4.8 m × 4.8 m window.

The lamination of the composite material, with dimensions outlined in Fig. 23, was performed at Madico [22], where a sheet 400 m long was produced.

At JLab rectangles were cut out of the laminated sheet, each 1.6 m wide and 4.8 m long. To form the final 4.8 m × 4.8 m single LTCC window, three of the rectangles were seamed together using G/Flex 655 epoxy. Additional window material was used to cover the nose, using the same seam. The seam was load tested to withstand a pressure 10 times higher than that expected from the C_4F_{10} gas flow and gas weight.

3.10.1. Window installation and gas leak tests

The installation of the window onto the box was achieved through gluing the window on the box sides using G/Flex 655 epoxy. The width of the window attached with glue was 12 cm, to provide sufficient gluing area. A photograph of the downstream window after installation is shown in Fig. 24.

After curing of both the upstream and downstream windows, the LTCC box was filled with nitrogen gas to a positive differential pressure of 2 in of water. Freon gas was pumped into the box and leak-checking was carried out using a refrigerant leak detector. After the leaks were sealed, the box was pressurized for a 48 h period to test the overall box gas tightness. This procedure was repeated after every movement of the LTCC boxes, as small shifts of the frame walls had the potential to introduce additional leaks due to the large surface area of the detector.

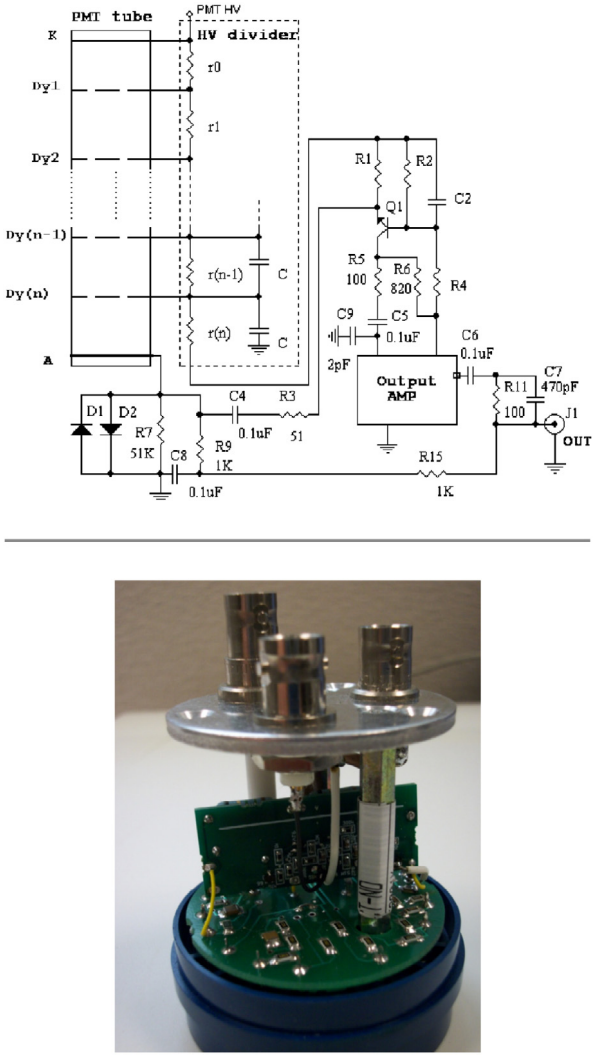

Fig. 21. Top: schematic of the PMT amplifier board, shown as a resistor chain for simplicity. The amplifier, designed to operate at currents from 0.7 to 1.5 mA, provides amplification in the first stage using a common base amplifier, made of a fast NPN transistor NE68033 by California Eastern Laboratories. In the output stage a PNP-NPN transistor is used. Bottom: the prototype module installed in the XP4500B PMT base. The bottom of the base has been modified to contain the high voltage input and the two output signals.

4. Electronics and readout

Fig. 25 shows a schematic diagram of the electronics and readout used for the LTCC detector. Since the magnetic shield case is near the bulb of the PMT, and the WC is in direct contact with the bulb, the electrons in the PMT could strike the inner bulb wall if the negative voltage was applied to the cathode. For this reason the signals are capacitatively coupled to positive HV, with the PMT cathode at ground potential. The XP4500B Photonis PMTs anodes are powered with positive polarity by a CAEN SY4527 high voltage mainframe outfitted with 1501P boards. There are two anode signals from the PMT output. One of them is connected directly to flash ADC boards built at JLab, the Flash ADC module FADC250 [23]. The FADC250 sampling frequency is 250 MHz. The other signal is discriminated by the JLab-built discriminator scaler module DSC2 [23], and connected to CAEN v1190 TDC modules. The TDCs have a 50 ps/channel timing resolution, and the discriminator threshold was set to 30 mV, corresponding to 15% of the SPE amplitude. The LTCC FADC250 and TDC information are read out using the CLAS12 Data Acquisition (DAQ) system [23].

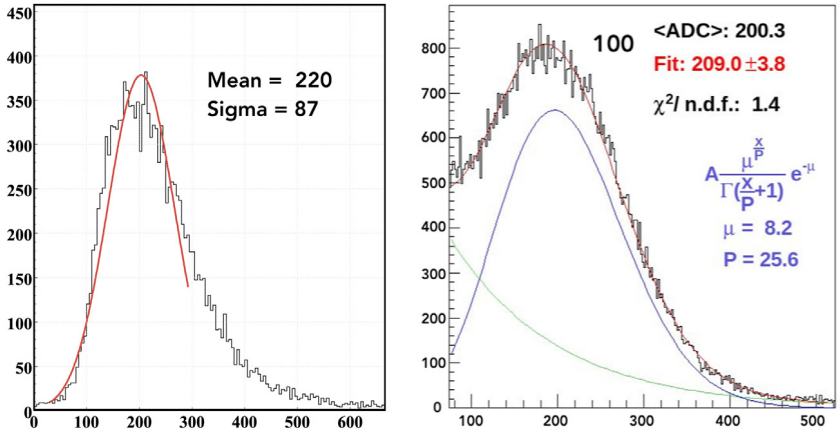

Fig. 22. The single photoelectron FADC spectrum of one of the PMTs with the modified base (left) compared with the original ADC output in the configuration of a dedicated external splitter and amplifier (right).

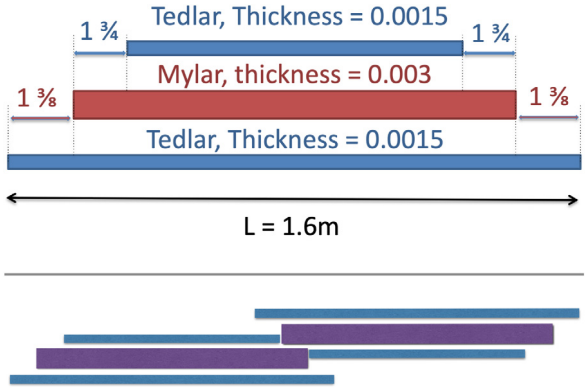

Fig. 23. Top: the design of the LTCC Tedlar/Mylar/Tedlar window sandwich. The pyramid design allowed for the seaming shown at the bottom. Bottom: the seaming design involves gluing Mylar to Mylar to ensure that the window stress is transmitted entirely to the Mylar.

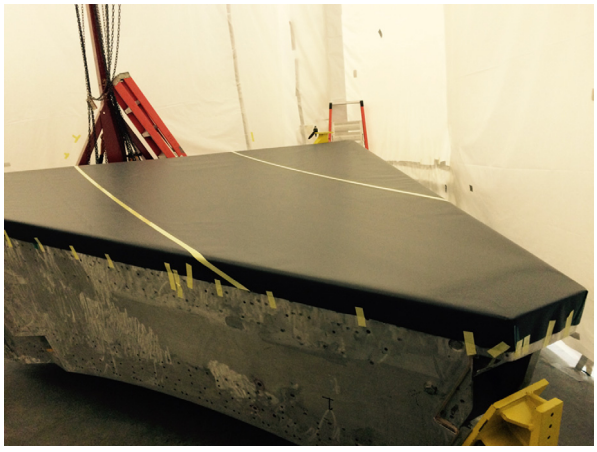

Fig. 24. The downstream window of one LTCC sector during curing of the epoxy. The two visible strips protect the window seaming.

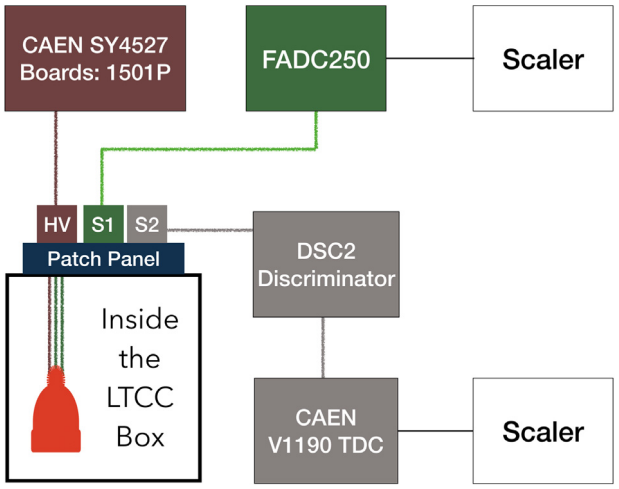

Fig. 25. The electronics schematic of the LTCC. One HV and two readout signals are connected from each PMT base to the patch panel. The patch panels then connect the HV to the CAEN SY4527 (1501P boards) and the PMT signals to the FADC250s and the DSC2 discriminators.

A typical signal from the FADC250 module is shown in Fig. 26. The signal is usually contained in 3 to 5 time samples (each time sample is 4 ns). In order to be written to tape, at least one of the 100 signal samples in the 400-ns wide readout window must be above a threshold of 30 channels, corresponding to about 30% of the SPE peak value. This is well above the typical pedestal variation of 1–5 channels. The FADC250 then integrates the FADC signal over a time window of 16 ns (4 samples) before the threshold crossing time, for the duration of 20 samples (80 ns). The final integrated charge used in the reconstruction code is the signal integral minus the electronic pedestal, as described in Fig. 26.

5. Hardware components summary

The hardware components of the LTCC are summarized in Table 2 and the electronics properties are summarized in Table 3.

6. Calibration

The calibration of the LTCC detector consists of matching the gains of the 216 PMTs. The main reason for this is that the FADC250 thresholds and sampling acquisition parameters are the same for all channels.

This gain calibration is carried out by using data with an electron beam incident on the experiment target. A random trigger is saved in the data stream at a rate of 100 Hz. This data subset includes LTCC events with PMT noise above the FADC pedestal, containing the single photoelectron signal (SPE).

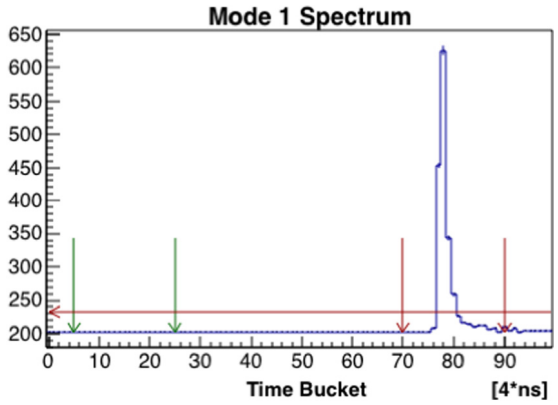

Fig. 26. The FADC250 digitized output as a function of sample index for one of the LTCC PMTs. The DAQ system saves a 400 ns time window (100 samples) if at least one of the 100 signal samples is above a 30-channel threshold. The integral signal is the sum of the output at the sample indexes between the two right arrows, one placed 4 samples before the signal crosses the threshold, and the other placed 20 samples after that. The final integrated charge used in the reconstruction code is this integral minus the pedestal. The pedestal is calculated using the average of the signal between the left arrows. The absolute positions of the pedestal acquisition limits and the relative position of the signal integration limits are adjusted in the DAQ parameters and loaded before each run.

Table 2
Summary of the LTCC component properties. For the mirror dimensions: L = length, W = width, T = thickness.

Property	Value
Mirrors	
Support structure	Kevlar/vinyl
Elliptical mirrors	L: 6–55″, W: 8–11″, T: 0.5″
Hyperbolic mirrors	L: 12–30″, W: 8–9.25″ T: 0.5″
Cylindrical Mirrors	L: 6″, W: 6–8″, T: 0.04″
Mirror coating	Al + MgF_2
Reflectivity	85% from 250 to 650 nm
Gas system	
Gas used	C_4F_{10}
Refraction index	1.00134
Transparency	100% above 220 nm
Density	9.94 kg/m^3
Window material	Tedlar/Mylar/Tedlar
Magnetic shields	
Eagle AAA material	80% Ni, 4% Mo, 15% Fe
Attenuation factor	85 Axial, 390 Transverse
PID	
π/K separation	3.5 to 9 GeV
Time resolution	0.6 ns

Table 3
Summary of the LTCC electronics.

Property	Value
PMTs	200 Photonis XP 4500B8 16 Photonis XP 4508
Voltage dividers	Photonis VD305K
HV mainframe	CAEN SY4527
HV boards	CAEN 1501P
Flash ADC	JLab FADC250-MHz [23]
TDC	CAEN 1190
Discriminators	DSC2 [23]

At the beginning of each experiment the PMT high voltages are adjusted to align the peak positions to a particular ADC value of $ADC_{SPE} = 200$. An example of the gain matching is shown in Fig. 27. The ADC spectra (see for Fig. 28 for typical histograms) are fit to identify the SPE peak positions. During analysis of physics events, the reconstructed number of photoelectrons for the digitized ADC value is calculated to be ADC/ADC_{SPE}.

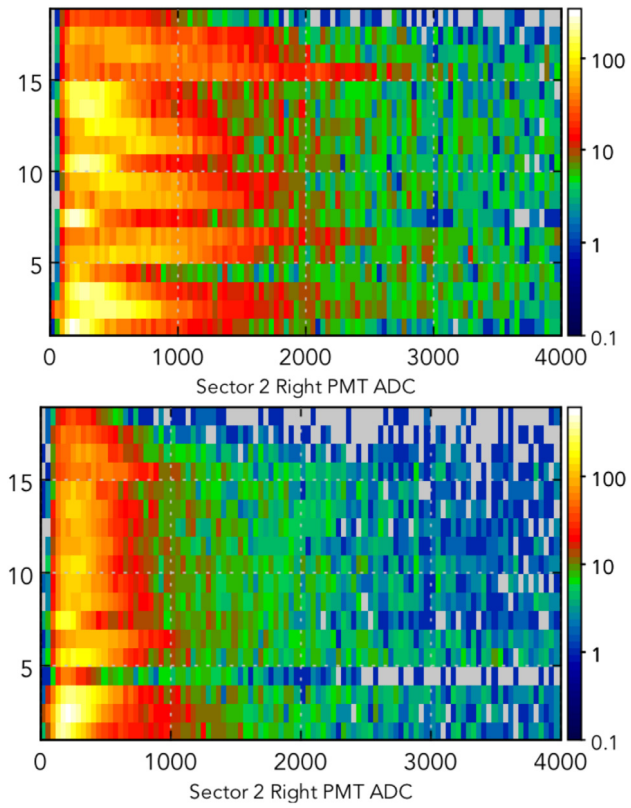

Fig. 27. Plot of PMT number vs. ADC for the LTCC sector 2 right side PMTs. The data is from the first production run in spring 2018. Top: before gain matching the SPE peak positions are not uniformly aligned at $ADC_{SPE} = 200$. Bottom: after gain matching the PMT responses are well aligned.

7. Reconstruction

The aim of the LTCC is to differentiate between pions and kaons. The lighter pions leave a signal in the detector, while the heavier kaons pass through the detector without leaving a signal. To accomplish this, it is necessary to associate the hits in the detector with their corresponding tracks from the drift chamber reconstruction. On average, the Cherenkov light from a charged particle will be collected by between 1 and 3 adjacent PMTs. The task of the reconstruction program is therefore to (a) cluster together the hits that belong to a single track and (b) provide the positional information needed to match the cluster with the correct reconstructed track. The reconstruction program is implemented as an engine in the CLAS12 event reconstruction framework [24].

7.1. Clustering algorithm

The Cherenkov cone associated with a charged particle is contained within a single, light-tight module of the LTCC. This allows for a relatively straightforward clustering algorithm:

1. Scan for the highest multiplicity hits, identified as the cluster center;
2. Grow the cluster by adding all hits adjacent to the cluster center within this sector;
3. Repeat the procedure until all hits have been assigned to a cluster.

7.2. Track matching

The *true* cluster center can be defined as the position where the charged particle (and its Cherenkov cone) crossed the elliptical mirror

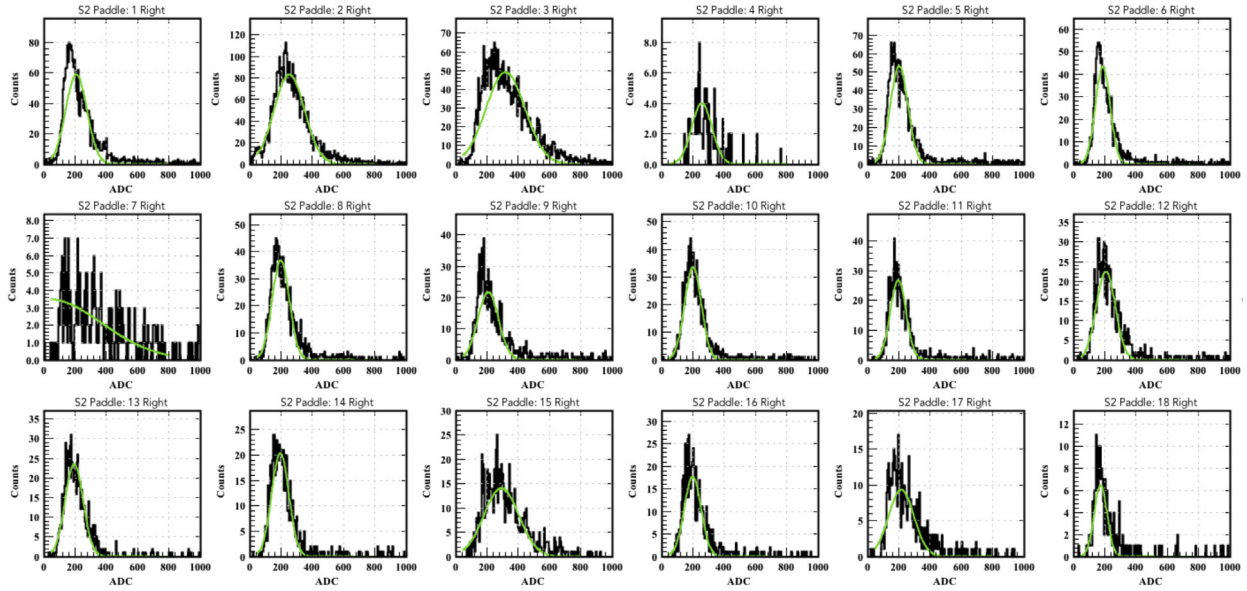

Fig. 28. The LTCC sector 2 right side ADC spectra. The data is from the first production run in spring 2018. The SPE peak positions are fit with a Gaussian function and the mean ADC_{SPE} parameters are recorded in the calibration database. The reconstructed number of photoelectrons for the digitized ADC value is ADC/ADC_{SPE}. Some anomalous PMTs can be seen: #4 and #7 show reduced rates due to non-optimal thresholds and gains.

of the LTCC. Due to the geometry of the LTCC, this position does not uniquely correspond to a single PMT, as the angle with which a particle crosses the elliptical mirrors depends on the particle momentum, position, charge, and the torus magnetic field and polarity. The implies that, based solely on the LTCC hits, the *true* cluster position cannot be uniquely constrained. This is illustrated in Fig. 29 where two particles hitting the same mirrors at different angles emit Cherenkov light that ends up being focused onto two different PMTs.

In order to perform the matching between the LTCC hit and the reconstructed drift chamber track, the estimated *true* cluster position is recalculated for each track, leveraging the Monte Carlo simulation of the LTCC to correctly associate a tentative *true* cluster position with the measured hits. The track that passes the closest to the tentative *true* cluster position is then chosen as the true match for this cluster.

8. Simulation

A realistic model of the LTCC has been developed, describing the location and material composition of the support box, mirrors, PMTs, Winston cones, magnetic shields, C_4F_{10} gas, and optical properties of the gas, mirrors, and WCs as a function of wavelength [17].

As part of the re-scoping of the CLAS Cherenkov detector to detect pions (both positive and negative) instead of negatively charged electrons, the optics of the mirrors had to be tuned in order to optimize the LTCC response for the angles of incidence for both charges. This was accomplished by aligning the mirrors using straight tracks (photons) originating from the target (placed at the center of the CLAS12 coordinate system), (see Section 3.6).

The efficiency of light collection, critical for LTCC operation, is tied into precise mirror positioning. The simulation has all of the details that allowed for all final decisions to be made for the LTCC optics design, including the mathematical outline of the mirror shapes and the placement of the optics focal points at the target (common to all mirrors) and at the centers of the faces of the PMTs.

8.1. Run period variations

At the start of CLAS12 beam operations, there was insufficient C_4F_{10} gas to fill all sectors, so some LTCC sectors were removed from the Forward Carriage. As they were installed or removed, any detected gas leaks were found and fixed. These CLAS12 configuration changes are imported in GEMC as database variations of the simulation setup. The default simulations only include sector 2 (S2), S3, S5, and S6, as the RICH detector [5] replaces the LTCC box in S4 (and a second RICH detector will be installed in the S1 position in the near future). The variations are listed in Table 4.

Table 4
LTCC simulation variations for different CLAS12 run periods. Shown are the configurations of the LTCC boxes in the different sectors of the CLAS12 Forward Carriage for each run period and the gas that was used to fill the detectors.

Run period	Sectors installed and gas
Default	S2, S3, S5, S6, all C_4F_{10}
Spring 2018	S2, S3, S6 (N_2), S5 (C_4F_{10})
Fall 2018	S3 (C_4F_{10}), S5 (N_2)
Spring 2018	S3 (C_4F_{10}), S5 (C_4F_{10})

9. Performance

The response of the LTCC to electrons and pions has been studied using experimental data from the spring 2019 run period, the first time that the LTCC S3 and S5 boxes were filled with C_4F_{10} gas. At the time of this writing the data is not yet fully calibrated. However, the CLAS12 detectors are sufficiently well calibrated to understand several fundamentals aspects of the LTCC response.

9.1. LTCC response to electrons

The electrons are selected using the reconstruction algorithms [24] that identify electron tracks. The LTCC response is calculated by checking whether or not the electrons produced a signal in the detector. The electron momenta has been selected in the expected pion response range, between 3.5 and 8 GeV. The criteria for event selection are:

- electrons identified using the reconstruction Event Builder algorithm;
- electrons must be within the geometrical fiducial volume of the LTCC.

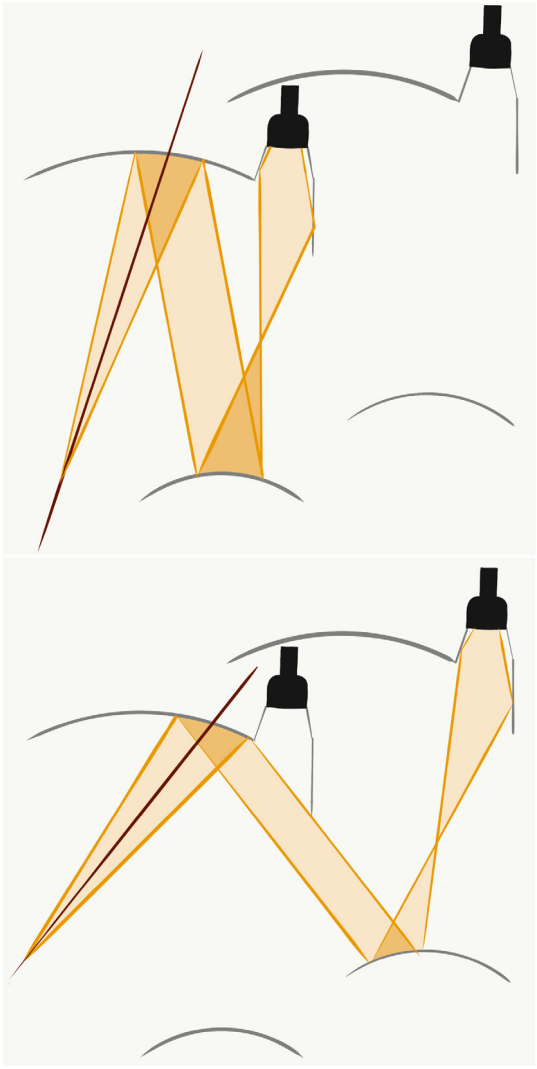

Fig. 29. Two different simulated LTCC hits for particles passing through the same elliptical mirror. Based on particle kinematics, either the PMT in the same segment (top) or a neighboring segment (bottom) is hit.

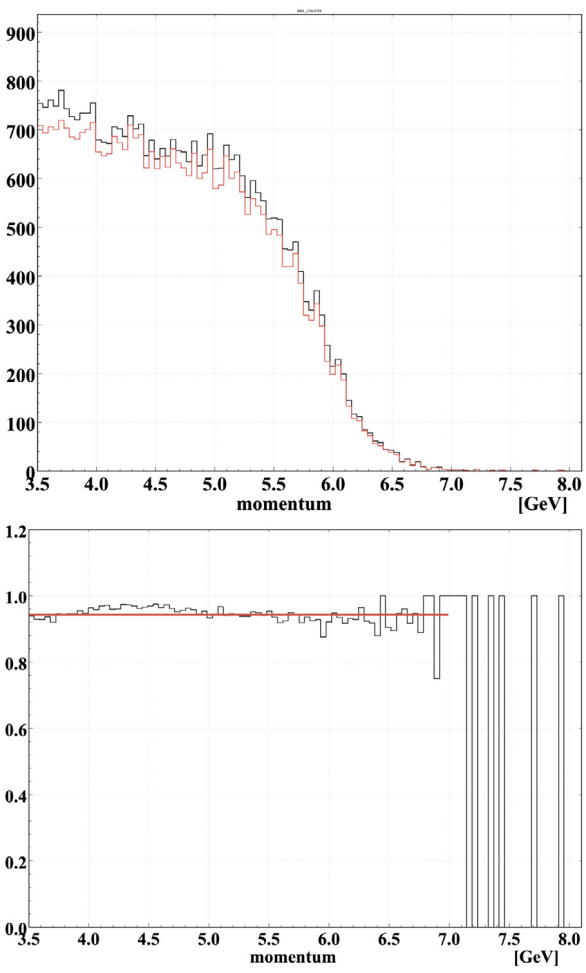

Fig. 30. Top: the number of reconstructed electrons vs. momentum (GeV) before and after the requirement of an associated LTCC signal. Bottom: the LTCC efficiency to electrons is the ratio of the two distributions above. A 0th-order polynomial fit gives an average of 94% efficiency.

The electron momentum spectrum before and after the requirement of an associated LTCC signal is shown in Fig. 30, along with the fit using a constant up to 7 GeV. The average efficiency for detection of electrons in the LTCC is 94%, slightly below the expected efficiency of 99%. This may be due to several reasons:

- the electron selection was not refined by using the calorimeters (due to the uncalibrated detector status);
- possible impurities in the gas, which was not purified by the recovery system (unavailable at that time);
- the data analyzed were not fully calibrated at the time of this writing;
- the mirror overlaps and repositioning issues mentioned in Section 3.6.1.

9.2. LTCC response to pions

The determine the response of the LTCC to pions, reconstructed positively charged pions were selected and a check was done on whether they produced a good signal in the LTCC detector. The positive pion selection considers all positively charged particles that pass a neutron missing mass cut for the reaction $ep \rightarrow e'\pi^+ n$. The criteria for event selection are:

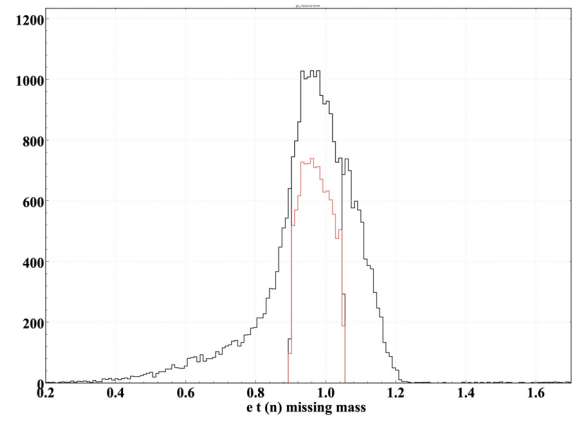

Fig. 31. The missing mass from the reaction $ep \rightarrow e'\pi^+ X$, where the peak at the neutron mass between 0.95 and 1.05 GeV is selected for the LTCC efficiency analysis. The positive pion candidates that satisfy the cuts are shown in black. The pions associated with an LTCC signal are shown in red. (For interpretation of the references to color in this figure legend, the reader is referred to the web version of this article.)

- the electron selection described in Section 9.1;

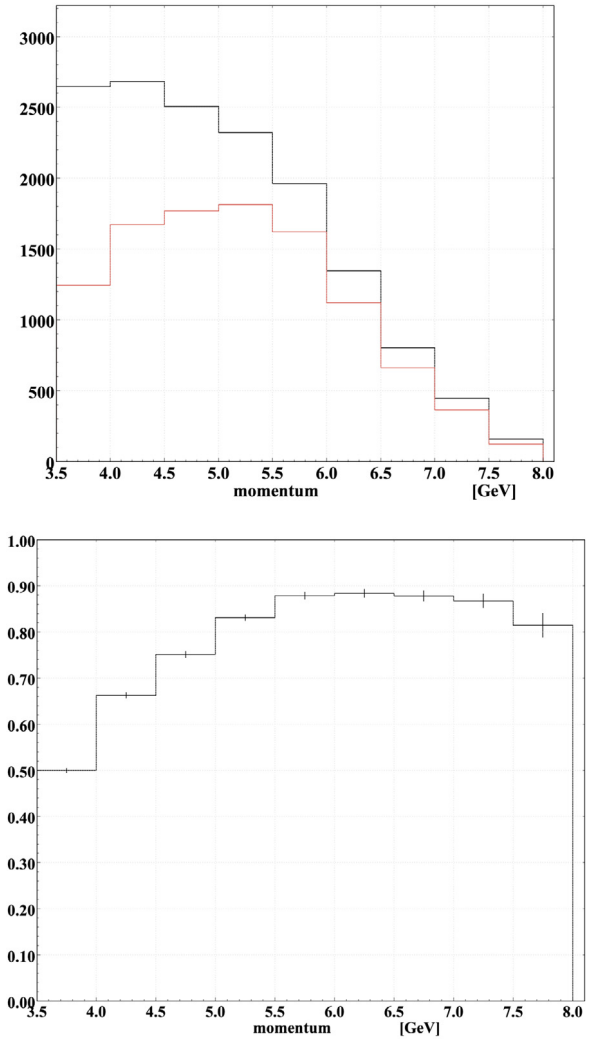

Fig. 32. Top: Histograms of the pion momentum distribution before (black) and after (red) the requirement of an associated LTCC signal. Bottom: The LTCC pion efficiency as a function of momentum given by the ratio of the top plot histograms normalized by the average electron efficiency of 94% shown in Fig. 30. (For interpretation of the references to color in this figure legend, the reader is referred to the web version of this article.)

- positive pion candidates are identified using the reconstruction Event Builder algorithm;
- the positive pion candidates must be within the LTCC geometrical fiducial volume;
- a neutron missing mass cut is applied between 0.9 and 1.05 GeV (see Fig. 31).

The missing mass cut is shown in Fig. 31. The positive pion candidates that satisfy the cuts are shown in black and those with a good LTCC cluster associated with the track are shown in red.

The momentum distribution of the pions is shown in Fig. 32 (top) for all pions and for the pions with an associated signal in the LTCC. The ratio, normalized by the electron efficiency of 94% found above to account for other system inefficiencies, defines the LTCC pion detection efficiency as a function of momentum and is shown in Fig. 32 (bottom). The LTCC response starts around 50% near the expected signal threshold of ~3.5 GeV and rises with momentum as expected, given that the number of emitted photons increases with momentum. A plateau of 88% is reached at a momentum of 5 GeV. This is within range of an expectation of the expected efficiency above 90%.

Fig. 33. The LTCC sectors installed after refurbishment on the CLAS12 Forward Carriage. The RICH detector is installed in the sector 4 position and the sector 1 position awaits the installation of a second RICH detector.

10. Conclusions

To address the change of its scope from electron to pion identification for momenta greater than 3.5 GeV, the original CLAS Cherenkov Counters were refurbished at part of the new CLAS12 Low Threshold Cherenkov Counter (LTCC) system. The work included significant improvements of the reflectivities for the mirrors and the Winston cones, p-terphenyl coating of the PMTs, expansion of the gas volumes, and redesign of the box walls and patch panels. The refurbishment aimed at increasing the number of photoelectrons in the response signal, which is considerably lower for pions compared to electrons. The LTCC detector sectors after refurbishment are shown in Fig. 33 installed on the CLAS12 Forward Carriage upstream of the Forward Time-of-Flight system [6]. The average LTCC efficiency for electron detection in the momentum range from 3.5 to 6.5 GeV is 94%. The pion efficiency starts around 50% near the expected signal threshold, and rises with momentum as expected. A plateau of 88% is reached at a momentum of 5 GeV. This is within range of an expectation of efficiency above 90%. Additional future studies are required to full quantify the detection efficiency of the CLAS12 LTCC for both positive and negative pions as a function of momentum.

Acknowledgments

We thank the Detector Support Group at Jefferson Lab for the work on the cone refurbishment, reflectivity tests, PMT divider modifications and installation, and for designing the gas control system and associated software. We thank Temple University for the p-terphenyl deposition. We thank Vladimir Popov for the implementation of the divider base modification. We thank the technical team of Hall B for their work and dedication on all aspects of the project. Finally, we thank all the Hall B staff for their unyielding support. This work was supported in part by DOE, USA Contract DE-AC05-06OR23177.

References

[1] V.D. Burkert, et al., The CLAS12 spectrometer at jefferson laboratory, Nucl. Instrum. Methods A (2020) in press (see this issue).

[2] R. Fair, et al., The CLAS12 superconducting magnets, Nucl. Instrum. Methods A (2020) in press (see this issue).

[3] M.D. Mestayer, et al., The CLAS12 drift chamber system, Nucl. Instrum. Methods A (2020) in press (see this issue).

[4] Y.G. Sharabian, et al., The CLAS12 high threshold cherenkov counter, Nucl. Instrum. Methods A (2020) in press (see this issue).

[5] M. Contalbrigo, et al., The CLAS12 ring imaging cherenkov detector, Nucl. Instrum. Methods A (2020) in press (see this issue).

[6] D.S. Carman, et al., The CLAS12 forward time-of-flight system, Nucl. Instrum. Methods A (2020) in press (see this issue).

[7] G. Asryan, et al., The CLAS12 pre-shower Calorimeter, Nucl. Instrum. Methods A (2020) in press (see this issue).

[8] M.A. Antonioli, et al., The CLAS12 silicon vertex tracker, Nucl. Instrum. Methods A (2020) in press (see this issue).

[9] F. Bossu, et al., The CLAS12 micromegas tracker, Nucl. Instrum. Methods A (2020) in press (see this issue).

[10] D.S. Carman, et al., The CLAS12 central time-of-flight system, Nucl. Instrum. Methods A (2020) in press (see this issue).

[11] P. Chatagnon, et al., The CLAS12 central neutron detector, Nucl. Instrum. Methods A (2020) in press (see this issue).

[12] M. Battaglieri, et al., The CLAS12 forward tagger, Nucl. Instrum. Methods A (2020) in press (see this issue).

[13] G. Adams, et al., The CLAS cherenkov detector, Nucl. Instrum. Methods A465 (2001) 414–427, http://dx.doi.org/10.1016/S0168-9002(00)01313-9.

[14] CLAS12 technical design report, 2008, https://www.jlab.org/Hall-B/clas12_tdr.pdf.

[15] I.M. Frank, I.E. Tamm, Coherent visible radiation of fast electrons passing through matter, C. R. Acad. Sci. URSS 14 (3) (1937) 109–114, doi: 10.1007/978-3-642-74626-0_2, 10.3367/UFNr.0093.196710o.0388, [Usp. Fiz. Nauk93, no.2, 388(1967)].

[16] Evaporated Coatings Inc., URL https://www.evaporatedcoatings.com.

[17] M. Ungaro, et al., The CLAS12 geant4 simulation, Nucl. Instrum. Methods A (2020) in press (see this issue).

[18] Photonis, photomultiplier tubes Catalog, 2007.

[19] P. Koczon, A. Braem, C. Joram, P. Solevi, M. Dürr, C. Höhne, Wavelength-Shifting Materials for the Use in RICH Detectors - P-Terphenyl and Tetraphenyl-Butadiene Revisited, Tech. Rep. PH-EP-Tech-Note-2012-003, CERN, Geneva, 2010, URL https://cds.cern.ch/record/1457653.

[20] S. Joosten, E. Kaczanowicz, M. Ungaro, M. Rehfuss, K. Johnston, Z.E. Meziani, Enhanced UV light detection using a p-terphenyl wavelength shifter, Nucl. Instrum. Methods A870 (2017) 110–115, http://dx.doi.org/10.1016/j.nima.2017.06.050, arXiv:1611.03467.

[21] V. Popov, Design and study of photomultiplier pulse-shaping amplifier powered by the current flowing through a voltage divider, Nucl. Instrum. Methods A505 (2003) 316–319, http://dx.doi.org/10.1016/S0168-9002(03)01076-3.

[22] Madico Inc. URL https://madico.com/about.

[23] S. Boyarinov, et al., The CLAS12 data acquisition system, Nucl. Instrum. Methods A (2020) in press (see this issue).

[24] V. Ziegler, et al., The CLAS12 software framework and event reconstruction, Nucl. Instrum. Methods A (2020) in press (see this issue).